CHEMISTRY
A EUROPEAN JOURNAL

DOI: 10.1002/chem.201002341

Flexibility and Sorption Selectivity in Rigid Metal–Organic Frameworks: The Impact of Ether-Functionalised Linkers

Sebastian Henke,[a] Rochus Schmid,[a] Jan-Dierk Grunwaldt,[b] and Roland A. Fischer*[a]

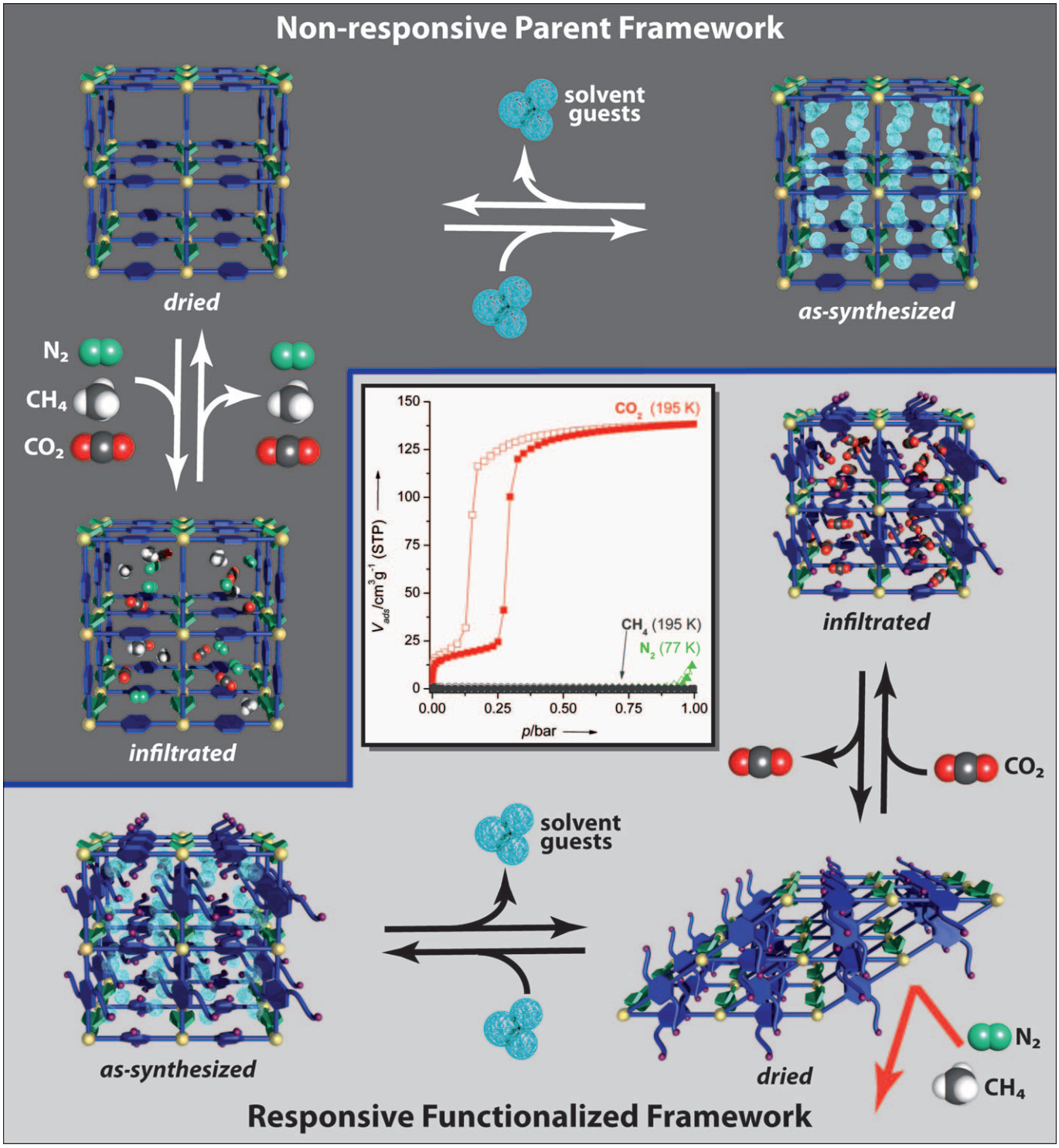

Abstract: The functionalisation of well-known rigid metal–organic frameworks (namely, $[Zn_4O(bdc)_3]_n$, MOF-5, IRMOF-1 and $[Zn_2(bdc)_2(dabco)]_n$; bdc = 1,4-benzene dicarboxylate, dabco = diazabicyclo[2.2.2]octane) with additional alkyl ether groups of the type -O-$(CH_2)_n$-O-CH_3 (n = 2–4) initiates unexpected structural flexibility, as well as high sorption selectivity towards CO_2 over N_2 and CH_4 in the porous materials. These novel materials respond to the presence/absence of guest molecules with structural transformations. We found that the chain length of the alkyl ether groups and the substitution pattern of the bdc-type linker have a major impact on structural flexibility and sorption selectivity. Remarkably, our results show that a high crystalline order of the activated material is not a prerequisite to achieve significant porosity and high sorption selectivity.

Keywords: carbon dioxide separation · metal–organic frameworks · polymers · selective sorption · structural flexibility

Introduction

Metal–organic frameworks (MOFs) are an emerging class of crystalline porous hybrid materials consisting of inorganic building blocks (e.g., metal clusters or metal–oxo clusters), which are interconnected by organic sub-units, the so-called linkers.[1,2] Their high specific pore volumes and surface areas together with tailored chemical functionality are interesting for a huge variety of applications, such as gas storage,[1,3] sensing,[4] separation,[5] catalysis[6] and medical applications.[7] In general, two families of MOF materials can be distinguished. 1) Firstly, there are many MOFs that feature robust and rigid networks. The full retention of the framework structure after desorption of solvent molecules (activation) and subsequent reversible adsorption/desorption cycles of other guests is a highly desired property.[1,3,8] 2) Secondly, there are soft MOFs, which exhibit pronounced framework dynamics. This feature can be associated with responsiveness to adsorption of guest molecules with a reversible change in lattice parameters, space group symmetry or other structural and physical properties, such as spin states of metal ions.[9–11] Most known flexible MOFs are layer-based systems, in which two-dimensional layers of coordination polymers are interconnected in the third dimension with a bidentate pillar linker. However, flexible and responsive MOFs are relatively rare in the literature compared with the wide variety of known rigid frameworks. Recently, linker functionalisation was shown to influence and trigger responsiveness in MOFs.[12] In particular, the post-synthetic linker functionalisation of the layer-based MOF $[Zn_2(NH_2\text{-bdc})_2(dabco)]_n$ (NH_2-bdc = 2-amino-1,4-benzene dicarboxylate; dabco = diazabicyclo[2.2.2]octane) initiated a breathing behaviour.[13] Furthermore, the implementation of a special pillar linker, featuring flexible 2-hydroxyethoxy groups, in $[Cd_2(pzdc)_2L]_n$ (pzdc = 2,3-pyrazinedicarboxylate, L = 2,5-bis(2-hydroxyethoxy)-1,4-bis(4-pyridyl)benzene) initiated high sorption selectivity for small polar molecules.[14]

Herein, we present our related results of turning known rigid and non-selective MOFs into responsive isoreticular derivatives. Ultra-high sorption selectivity towards CO_2 over N_2 and CH_4 was initiated by choosing flexible ether side groups of the type -O-$(CH_2)_n$-O-CH_3 (n = 2, 3 or 4), which are covalently bound to the phenyl ring of the dicarboxylate linker. We found that both the alkyl chain length and the substitution pattern at the phenyl ring have a major impact on flexibility as well as sorption selectivity of the MOFs. To demonstrate the general applicability of our concept, we have chosen two well-known MOFs, namely, $[Zn_4O(bdc)_3]_n$ (also named MOF-5, IRMOF-1)[8] and $[Zn_2(bdc)_2(dabco)]_n$[15] (bdc = 1,4-benzene dicarboxylate) as examples. The novel ether-functionalised bdc-type linkers 2,5-bis(2-methoxyethoxy)benzene dicarboxylic acid (H_2L^1), 2,5-bis(3-methoxypropoxy)benzene dicarboxylic acid (H_2L^2), 2,5-bis(4-methoxybutoxy)benzene dicarboxylic acid (H_2L^3) and 2-(2-methoxyethoxy)benzene dicarboxylic acid (H_2L^4) were synthesised by Mitsunobu etherification[16] and then utilised in the MOF syntheses instead of conventional H_2bdc.

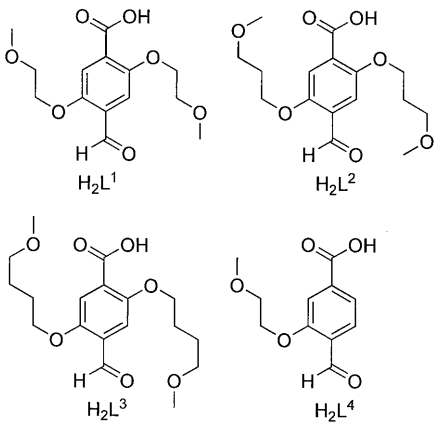

[a] S. Henke, Dr. R. Schmid, Prof. Dr. R. A. Fischer
Chair of Inorganic Chemistry II
Organometallics and Materials Chemistry
Ruhr-University Bochum, Universitätsstrasse 150
44780 Bochum (Germany)
Fax: (+49) 234-32-14174
E-mail: roland.fischer@rub.de

[b] Prof. Dr. J.-D. Grunwaldt
Chair for Chemical Technology and Catalysis
Institute for Technical Chemistry and Polymer Chemistry
Karlsruhe Institute of Technology
Engesserstrasse 20, 76131 Karlsruhe (Germany)

Supporting information for this article is available on the WWW under http://dx.doi.org/10.1002/chem.201002341.

Results and Discussion

Syntheses and characterisation: The ether-functionalised coordination polymers $[Zn_4O(L^X)_3(DMF)_m]_n$ and $[Zn_2(L^X)_2(dabco)(DMF)_m]_n$ ($X=1$, 2, 3 and 4) were synthesised in a solvothermal synthesis from $Zn(NO_3)_2 \cdot x H_2O$ ($x=4$ and 6) and the organic linkers in DMF (Figure 1). The implemented alkyl ether side-chain substituents are flexible and feature a polar methoxy head group. Hence, the functional groups introduce ether solvent like properties, but are fixed at the backbone of the porous parent network. The structural analogy of the functionalised frameworks was indicated by comparing the powder X-ray diffraction (PXRD) patterns of the as-synthesised materials with the calculated diffraction patterns of the unmodified parent MOFs (Figures 2 and 7).[8,15] Moreover, single-crystal X-ray structures of the as-synthesised materials $[Zn_4O(L^X)_3(DMF)_m]_n$ ($X=1$, 2, 3 and 4) and $[Zn_2(L^1)_2(dabco)(DMF)_m]_n$ were determined to analyse the molecular structure of the compounds in more detail (see the Supporting Information). As expected, it was not yet possible to refine the atom positions of the flexible ether chains in the single-crystal structure analysis due to high disorder. In fact, the structural features of the ether-functionalised MOFs can be viewed as a crystalline solid-state material combined with disordered liquid-state solvent properties.[17]

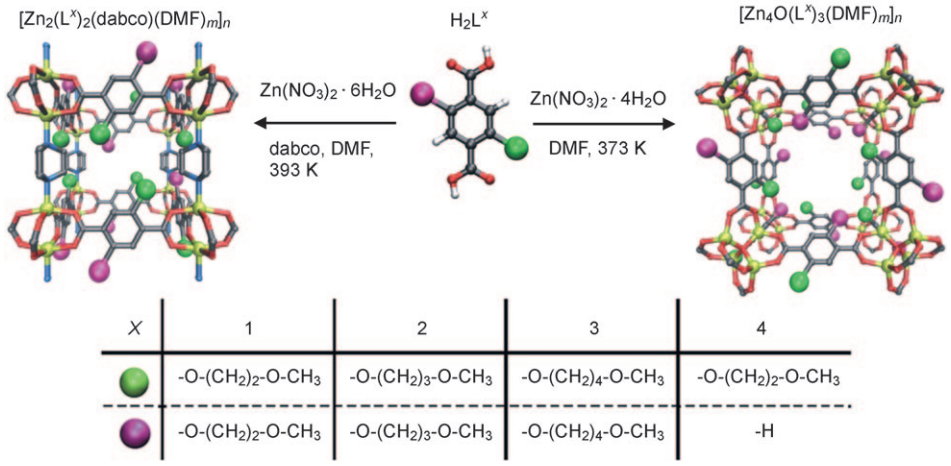

Figure 1. Solvothermal syntheses of ether-functionalised MOFs. Four different linkers, H_2L^X, were utilised in MOF syntheses to achieve eight different ether-functionalised frameworks $[Zn_2(L^X)_2(dabco)]_n$ and $[Zn_4O(L^X)_3]_n$ ($X=1$, 2, 3 and 4). Zinc, oxygen, nitrogen and carbon atoms are shown in yellow, red, blue and grey, respectively (hydrogen atoms and disordered solvent molecules were omitted for clarity).

The as-synthesised MOFs were activated by solvent exchange with chloroform and finally dried in vacuo to achieve the solvent-free materials $[Zn_4O(L^X)_3]_n$ and $[Zn_2(L^X)_2(dabco)]_n$ ($X=1$, 2, 3 and 4) according to standard procedures for the parent MOFs. The activated MOFs were analysed with thermogravimetric analysis (TGA), FTIR spectroscopy and ^{13}C-MAS-NMR (magic angle spinning) spectroscopy. Evidence of the expected stoichiometric presence of the functional groups inside the pores was given by elemental analysis, as well as high-resolution ^{1}H and ^{13}C NMR spectroscopy of digested MOF samples in DCl/D_2O/[D_6]DMSO (see the Supporting Information).

Structural dynamics of $[Zn_4O(L^X)_3]_n$ MOFs: Interestingly, the novel functionalised MOFs behave differently upon removal of the solvent guests from the pores. Surprisingly, the PXRD pattern of dried $[Zn_4O(L^1)_3]_n$ shows an almost X-ray amorphous material (Figure 2c). Only the first reflex at $2\theta=6.7°$ is present as a very small peak. This effect is much less pronounced for the other derivatives $[Zn_4O(L^X)_3]_n$ ($X=$ 2, 3 and 4). Moisture was rigorously ruled out by strictly working under an inert gas atmosphere (dried Ar; Schlenk and glovebox techniques). However, exposing the amorphous material $[Zn_4O(L^1)_3]_n$ to DMF vapour under reduced pressure quantitatively yielded the reinfiltrated material

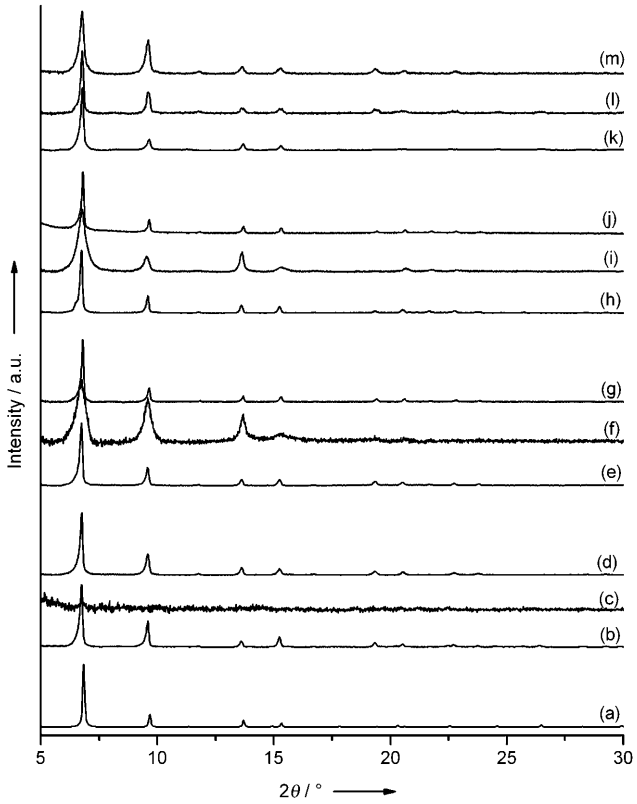

Figure 2. Powder X-ray diffraction (PXRD) patterns of $[Zn_4O(L^X)_3]_n$ ($X=1$, 2, 3 and 4): a) $[Zn_4O(bdc)_3]_n$ reference (simulated from the X-ray structure);[8] b) as-synthesised $[Zn_4O(L^1)_3(DMF)_m]_n$; c) dried $[Zn_4O(L^1)_3]_n$; d) reinfiltrated DMF@$[Zn_4O(L^1)_3]_n$; e) as-synthesised $[Zn_4O(L^2)_3(DMF)_m]_n$; f) dried $[Zn_4O(L^2)_3]_n$; g) reinfiltrated DMF@-$[Zn_4O(L^2)_3]_n$; h) as-synthesised $[Zn_4O(L^3)_3(DMF)_m]_n$; i) dried $[Zn_4O(L^3)_3]_n$; j) reinfiltrated DMF@$[Zn_4O(L^3)_3]]_n$; k) as-synthesised $[Zn_4O(L^4)_3(DMF)_m]_n$; l) dried $[Zn_4O(L^4)_3]_n$ and m) reinfiltrated DMF@-$[Zn_4O(L^4)_3]_n$.

DMF@$[Zn_4O(L^1)_3]_n$, which was again perfectly crystalline (Figure 2d), similar to the initial as-synthesised material $[Zn_4O(L^1)_3(DMF)_m]_n$. It is well known that the formation of crystalline IRMOFs can occur at room temperature in the liquid phase.[18] However, the reordering process reported herein is very different from such a room-temperature synthesis. Instead the structural transformation occurs depending on the absence or presence of guest molecules adsorbed in the pores of the framework.

Interestingly, the fully reversible crystalline-to-amorphous transformation appears also by repetitive infiltration and removal of other polar guest molecules such as *N*,*N*′-diethylformamide (DEF) and THF in the gas phase (Figure 3b and c). However, the recovery of crystallinity does not work by gas-phase infiltration of non-polar guest molecules, such as pentane or toluene, as analysed by PXRD (Figure 3d and e). PXRD analysis of the other ether-functionalised IRMOF derivatives $[Zn_4O(L^X)_3]_n$ ($X=2$, 3 and 4) in the course of activation and solvent reinfiltration cycles reveals the huge impact of the substitution pattern of the linker and the alkyl chain length. The PXRD pattern of the dried material, $[Zn_4O(L^2)_3]_n$, also indicates a substantial loss of crystallinity of the material upon solvent removal (Figure 2f). The X-ray reflexes of low *hkl* values are still visible as broad peaks in the diffraction pattern, suggesting that the loss in long-range order is not as far-reaching as in $[Zn_4O(L^1)_3]_n$. Again, the initial highly crystalline phase is recovered upon gas-phase infiltration of DMF in the pores (Figure 2g). Similar results can be concluded from the diffraction patterns of $[Zn_4O(L^3)_3]_n$ (Figure 2h–j). The loss in crystallinity upon removal of DMF from the pores is less apparent compared to $[Zn_4O(L^2)_3]_n$. Remember, the only difference between $[Zn_4O(L^1)_3]_n$, $[Zn_4O(L^2)_3]_n$, and $[Zn_4O(L^3)_3]_n$ is the number of CH_2 groups in the alkyl chain. However, the fourth IRMOF material $[Zn_4O(L^4)_3]_n$, which utilises linker L^4 with one ether side chain instead of two, displays no loss in crystallinity at all (Figure 2k–m). These results indicate an interesting new phenomenon in IRMOF chemistry. A more or less pronounced and fully reversible crystalline-to-amorphous phase transition can be triggered by the implementation of flexible methoxy-terminated alkyl groups and can be tuned by the alkyl chain length and the substitution pattern at the bdc-type linker.

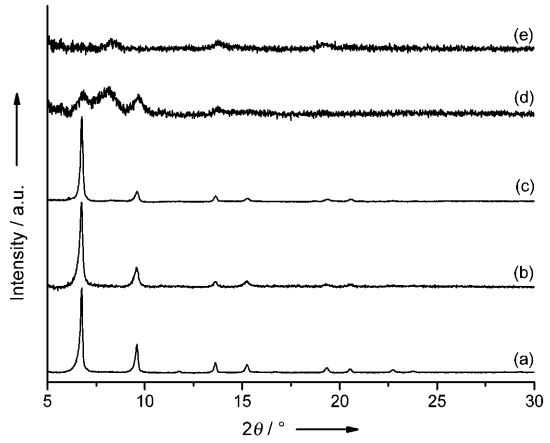

Figure 3. PXRD patterns of reinfiltrated samples of $[Zn_4O(L^1)_3]_n$: a) DMF@$[Zn_4O(L^1)_3]_n$; b) DEF@$[Zn_4O(L^1)_3]_n$; c) THF@$[Zn_4O(L^1)_3]_n$; d) pentane@$[Zn_4O(L^1)_3]_n$ and e) toluene@$[Zn_4O(L^1)_3]_n$.

In general, crystalline-to-amorphous phase transitions are known from other MOFs.[11,19] Interestingly, such effects were never reported for IRMOF-type structures, which are particularly known for rigidity and do not show any flexibility, even in the case of a huge variety of previously known linker-functionalised derivatives.[1,20] That rigidity is attributed to the symmetry of the inorganic sub-unit, which has less flexibility to allow framework dynamics.[10,21] However, our data surprisingly show that a suitably functionalised IRMOF structure can be responsive to the nature of guest in the pores.

Two different mechanisms are suggested to explain the reversible crystalline-to-amorphous phase transitions in $[Zn_4O(L^1)_3]_n$: 1) In the absence of any polar guest molecule, strong dipolar intermolecular interactions of the methoxy groups with each other may lead to a major displacement of the linkers and the $[Zn_4O]^{6+}$ framework nodes. 2) In the absence of any polar guest molecule, the methoxy groups coordinate to the zinc centres at the framework nodes and induce a random distortion of the $[Zn_4O]^{6+}$ cluster. Both mechanisms may lead to a significant loss of long-range order as a source of the phase transitions.

FTIR spectroscopy is a useful tool to analyse the coordination of the carboxylates to the zinc centres in the crystalline as well as in the amorphous states of $[Zn_4O(L^1)_3]_n$ in more detail.[22] A close-up view of the vibration bands between 400 and 2000 cm^{-1} of crystalline $[Zn_4O(L^1)_3(DMF)_m]_n$, amorphous $[Zn_4O(L^1)_3]_n$, pure DMF, protonated H_2L^1, and the potassium salt K_2L^1 is shown in Figure 4. The spectra of H_2L^1 and K_2L^1 represent the positions of the carboxylate stretching vibrations, if they are protonated and non-coordinating or if they are coordinating in a monodentate fashion to metal centres. No significant changes or shifts of the carboxylate stretching vibrations are visible in the spectra of the DMF-loaded MOF and the dried MOF. The additional vibration bands in the spectrum of $[Zn_4O(L^1)_3(DMF)_m]_n$ can be assigned to DMF molecules in the pores of the as-synthesised material. The splitting of the carbonyl vibration of DMF is assigned to interactions between the adsorbed DMF molecules and the framework. A comparison of the spectrum of $[Zn_4O(L^1)_3]_n$ with the spectrum of H_2L^1 indicates that no protonated carboxylates, similar to H_2L^1, are present in the dried material. The small shoulder at the asymmetric stretching vibration of the carboxylate groups (1548 cm^{-1}) in the spectrum of $[Zn_4O(L^1)_3]$ is in a similar position as for the asymmetric stretching vibration of K_2L^1. Therefore, some carboxylates of the dried MOF may only coordinate in a monodentate fashion to the zinc centres. However, the majority of the carboxylates still bind in the expected bidentate μ^2 coordination to zinc. Similar results can be concluded from the FTIR spectra of the other functionalised IRMOF

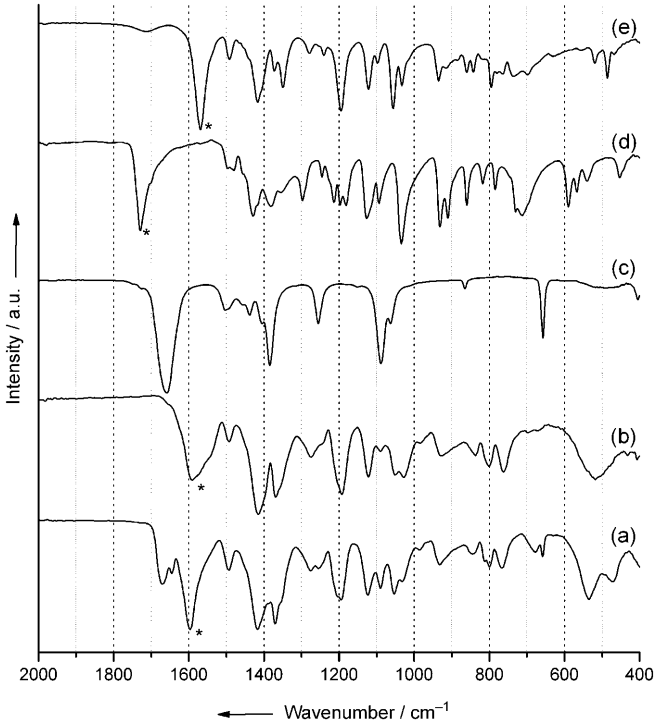

Figure 4. Attenuated total reflectance (ATR) FTIR spectra of a) as-synthesised $[Zn_4O(L^1)_3(DMF)_m]_n$, b) dried $[Zn_4O(L^1)_3]_n$, c) DMF, d) H_2L^1 and e) K_2L^1. The asymmetric stretching vibrations of the carboxylate groups are marked with an asterisk (*).

derivatives utilising linker L^2 and L^3 (see the Supporting Information).

A further hint for a reversible change in the zinc coordination sphere, depending on the presence or absence of DMF guests, is given by preliminary X-ray absorption near-edge structure (XANES) and extended X-ray absorption fine structure (EXAFS) data (see the Supporting Information). The XANES and EXAFS spectra are very similar before drying and after reinfiltration of DMF guests. They show a distortion of the $[Zn_4O]^{6+}$ tetrahedron upon solvent removal (see the Supporting Information for details). However, it is not yet possible to get unambiguous evidence for coordination of the flexible methoxy groups to the zinc atoms of the inorganic building block of the IRMOF derivative from the spectroscopic information obtained so far.

To get more information about the possible coordination of ether groups to the $[Zn_4O]^{6+}$ nodes of an IRMOF, we performed DFT calculations of simple model structures. Basic zinc formiate, $[Zn_4O(O_2CH)_6]$ (Figure 5, structure A), was employed as a structural model for the framework node of IRMOF-type structures. A distorted basic zinc formiate model structure, consisting of $[Zn_4O(O_2CH)_6]$ and two additional $(CH_3)_2O$ molecules (Figure 5, structure B), which are connected to one zinc atom of the $[Zn_4O]^{6+}$ cluster, is employed to get information about the binding of ether groups to the zinc atoms in comparison to the conventional basic zinc formiate model structure. We have chosen this distorted model structure because well-known literature examples of

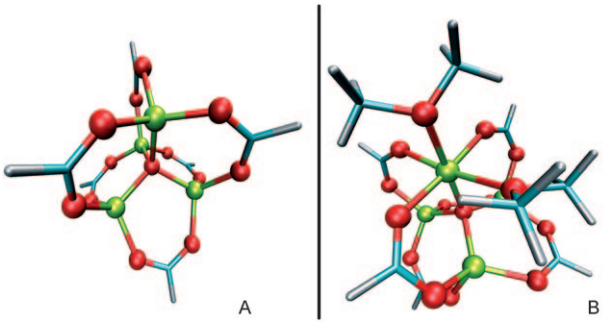

Figure 5. Representations of the calculated model structures: A) Basic zinc formiate $[Zn_4O(O_2CH)_6]$ and B) $[Zn_4O(O_2CH)_6(OMe_2)_2]$. Zinc, oxygen, carbon, and hydrogen atoms are shown in yellow, red, cyan, and silver, respectively.

$[Zn_4O(O_2C)_6]$-based MOFs feature one zinc atom per $[Zn_4O]^{6+}$ building unit with an octahedral coordination sphere, whereas the other three zinc atoms of the inorganic building block are tetrahedrally coordinated.[23] The additional ligands at the octahedrally coordinated zinc atoms of the literature reference structures are DEF or water solvent molecules from the MOF syntheses. Structure B is constructed similar to the framework nodes of the reference structures. Structure A was optimised in the T_d point group, whereas structure B was optimised with no symmetry constraints. For determination of the binding energy of dimethyl ether to basic zinc formiate, the structure of dimethyl ether was optimised in C_{2v} symmetry. To ensure that local minima were located, vibrational frequencies were calculated for all optimised structures.

The binding energy per dimethyl ether molecule to basic zinc formiate was calculated to be 15.1 kJ mol^{-1}. Therefore, a coordination of ether groups to the framework nodes of the activated MOFs seems to be feasible. Evaluation of structure B shows a remarkable distortion from the ideal octahedral coordination sphere (see the Supporting Information for further details). This distortion may be statistically initiated from several directions in the cubic structure, which may lead to a lack in long-range order and therefore an X-ray amorphous material. We suggest that such a distortion of the $[Zn_4O]^{6+}$ building block, initiated by additional coordination of some of the flexible methoxy groups of the linker, is the major reason for the crystalline-to-amorphous phase transition.

In the presence of polar guests, the ether side chains may interact with the guest molecules and also compete with them for weak coordination at Zn^{2+} sites (Figure 6). Clearly, the covalent anchorage of the ether side groups of optimum length at the linkers appears to be a prerequisite to trigger the observed effect. In summary, we attribute the amorphous-to-crystalline transition to a peculiar case of framework flexibility and not to an unspecific decomposition and breakdown of the framework upon solvent removal.

Structural dynamics of $[Zn_2(L^X)_2(dabco)]_n$ MOFs: A reversible crystalline-to-crystalline transformation was observed in

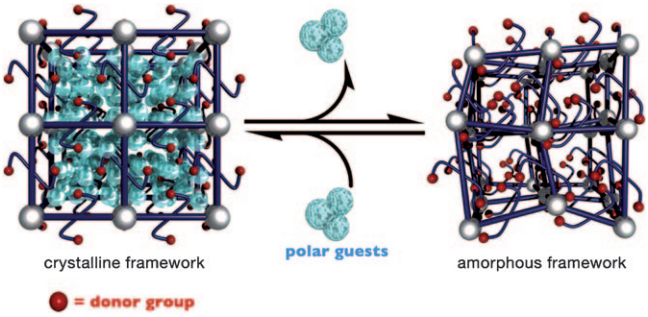

Figure 6. Representation of the reversible crystalline-to-amorphous transition in $[Zn_4O(L^1)_3]_n$. In response to the presence or absence of polar guest molecules, the framework reversibly switches between two states. Upon solvent removal some attached flexible methoxy groups may coordinate to the zinc centres, which induces a random distortion of the $[Zn_4O(O_2C)_6]_n$ building block leading to a vast deprivation in long-range translational order.

the case of the functionalised derivatives of $[Zn_2(bdc)_2(dabco)]_n$. The PXRD of dried $[Zn_2(L^1)_2(dabco)]_n$ (Figure 7d) shows a completely different pattern than the as-synthesised form $[Zn_2(L^1)_2(dabco)(DMF)_m]_n$ (Figure 7c). Some of the reflexes are shifted to higher 2θ values, indicating a remarkable contraction of the framework upon solvent or guest removal. This kind of framework breathing appears to be similar to the recently reported breathing of post-synthetic modified derivatives of $[Zn_2(NH_2\text{-}bdc)_2(dabco)]_n$ (NH_2-bdc = 2-aminobenzene dicarboxylate).[14] Gas-phase infiltration of DMF or EtOH molecules in the pores of $[Zn_2(L^1)_2(dabco)]_n$ yield the infiltrated composites DMF@$[Zn_2(L^1)_2(dabco)]_n$ and EtOH@$[Zn_2(L^1)_2(dabco)]_n$, which again feature the original open-pore phase (Figure 7e and f). Due to the saturated coordination sphere of the zinc centres in the $[Zn_2(L^1)_2(dabco)]_n$ (in contrast to the above cases $[Zn_4O(L^X)_3]_n$), the structural transformation must be based on interactions between the flexible ether groups and the framework backbone (similar to the structural transformation reported for the partially 2-propanol-loaded material $[Zn_2(bdc)_2(dabco)]_n$),[24] rather than a reversible coordination/uncoordination of the methoxy groups to the zinc centres. Interestingly, PXRD patterns of the dried materials $[Zn_2(L^2)_2(dabco)]_n$, $[Zn_2(L^3)_2(dabco)]_n$, and $[Zn_2(L^4)_2(dabco)]_n$ do not show this drastic framework breathing (Figure 7g–o). The diffraction reflexes shift only slightly in position relative to the reflexes of the as-synthesised materials. Therefore, our results again illustrate the major impact of the substitution pattern, as well as alkyl chain length, on the breathing behaviour of the "jungle-gym" type $[Zn_2(dicarboxylate)_2(dabco)]_n$ frameworks.

As-synthesised $[Zn_2(L^1)_2(dabco)(DMF)_m]_n$ crystallises in the *C*2/*m* space group as already determined by single-crystal diffraction (see the Supporting Information). Accordingly, the reflexes of the PXRD patterns of as-synthesised

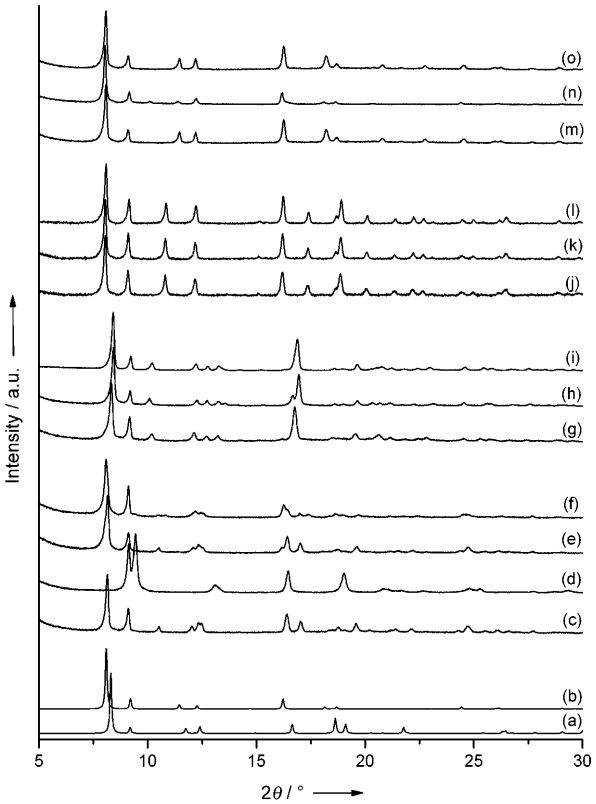

Figure 7. PXRD patterns of $[Zn_2(L^X)_2(dabco)]_n$ ($X = 1$, 2, 3 and 4): a) $[Zn_2(bdc)_2(dabco)(DMF)_m]_n$ reference (simulated from the X-ray structure);[15] b) $[Zn_2(bdc)_2(dabco)]_n$ reference (simulated from the X-ray structure);[15] c) as-synthesised $[Zn_2(L^1)_2(dabco)(DMF)_m]_n$; d) dried $[Zn_2(L^1)_2(dabco)]_n$; e) reinfiltrated DMF@$[Zn_2(L^1)_2(dabco)]_n$; f) reinfiltrated EtOH@$[Zn_2(L^1)_2(dabco)]_n$; g) as-synthesised $[Zn_2(L^2)_2(dabco)(DMF)_m]_n$; h) dried $[Zn_2(L^2)_2(dabco)]_n$; i) reinfiltrated DMF@$[Zn_2(L^2)_2(dabco)]_n$; j) as-synthesised $[Zn_2(L^3)_2(dabco)(DMF)_m]_n$; k) dried $[Zn_2(L^3)_2(dabco)]_n$; l) reinfiltrated DMF@$[Zn_2(L^3)_2(dabco)]_n$; m) as-synthesised $[Zn_2(L^4)_2(dabco)(DMF)_m]_n$; n) dried $[Zn_2(L^4)_2(dabco)]_n$ and o) reinfiltrated DMF@$[Zn_2(L^4)_2(dabco)]_n$.

$[Zn_2(L^1)_2(dabco)(DMF)_m]_n$, dried $[Zn_2(L^1)_2(dabco)]_n$, and reinfiltrated DMF@$[Zn_2(L^1)_2(dabco)]_n$ could be indexed in the monoclinic space group *C*2/*m*. To analyse the breathing mode in more detail, the cell parameters for the guest infiltrated and dried states of $[Zn_2(L^1)(dabco)]_n$ were refined (Table 1; see the Supporting Information for details). The (110) reflex at $2\theta = 8.1°$ is shifted to $2\theta = 9.5°$ when the guest molecules were removed from the pores. Accordingly the (200) reflex is shifted from $2\theta = 10.5°$ to $2\theta = 9.4°$, whereas the (001) reflex does not change its position (Figure 8). Corresponding to the refined cell parameters a structural model

Table 1. Results of the cell refinement of PXRD patterns of the different forms of $[Zn_2(L^1)_2(dabco)]_n$ in the monoclinic space group *C*2/*m*.

	a [Å]	*b* [Å]	*c* [Å]	α [°]	β [°]	γ [°]	*V* [Å^{-3}]
$[Zn_2(L^1)_2(dabco)(DMF)_m]_n$	16.75(3)	14.20(3)	9.75(1)	90	91.8(7)	90	2316(8)
$[Zn_2(L^1)_2(dabco)]_n$	18.90(4)	10.74(1)	9.66(1)	90	90.3(9)	90	1958(4)
DMF@$[Zn_2(L^1)_2(dabco)]_n$	16.70(5)	13.98(3)	9.63(2)	90	91.6(24)	90	2247(9)

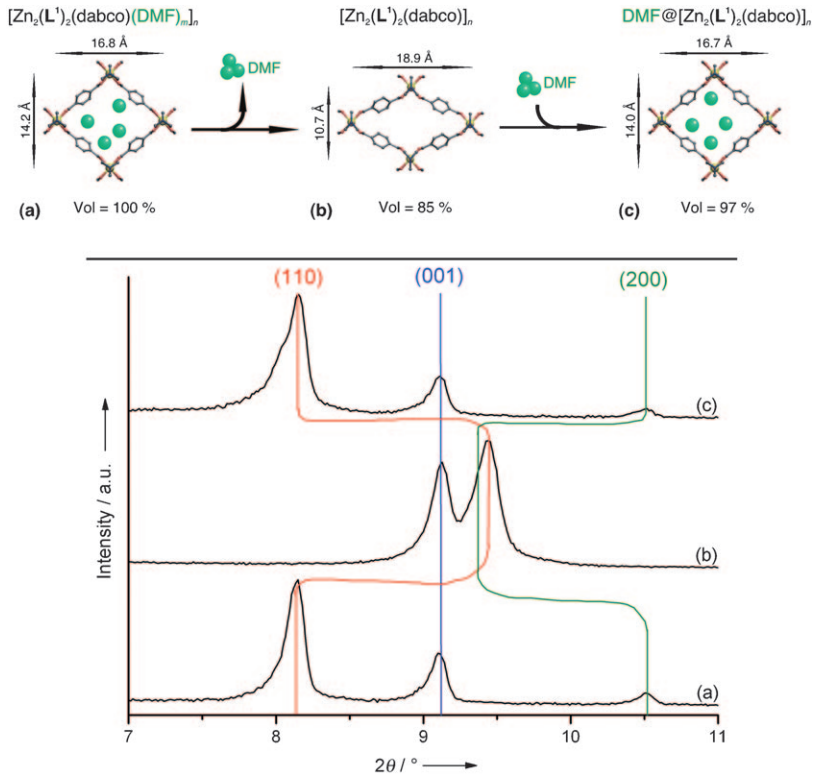

Figure 8. Close-up view of the PXRD patterns in the range from $2\theta = 7$–$11°$ (bottom) and structural models for the individual states of $[Zn_2(L^1)_2(dabco)]_n$ derived from cell refinement of the PXRD patterns (top): a) as-synthesised $[Zn_2(L^1)_2(dabco)(DMF)_m]_n$; b) dried $[Zn_2(L^1)_2(dabco)]_n$; c) reinfiltrated DMF@$[Zn_2(L^1)_2(dabco)]_n$. The flexible 2-methoxyethoxy side chains were not included in the model structures.

for the dried material $[Zn_2(L^1)_2(dabco)]_n$ could be derived (see the Supporting Information for details).

The open-pore phase $[Zn_2(L^1)_2(dabco)(DMF)_m]_n$ is transformed to a narrow-pore phase in $[Zn_2(L^1)_2(dabco)]_n$, which has only 85% of the cell volume of the initial open form. Subsequent re-adsorption of DMF in the pores of the dried, narrow-pore material transfers the MOF back to the open-pore structure DMF@$[Zn_2(L^1)_2(dabco)]_n$ (Figure 8).

Gas sorption properties: The separation of CO_2 from N_2 or CH_4 is of great relevance for industrial applications, for example, the capture of CO_2 from flue gas or CO_2/CH_4 separation for natural gas upgrading. To analyse the sorption abilities, N_2 (77 K), CO_2 (195 K) and CH_4 (195 K) sorption isotherms of $[Zn_4O(L^X)_3]_n$ and $[Zn_2(L^X)_2(dabco)]_n$ ($X = 1$, 2 and 4) were recorded (Figure 9). The materials $[Zn_4O(L^1)_3]_n$, $[Zn_4O(L^2)_3]_n$,

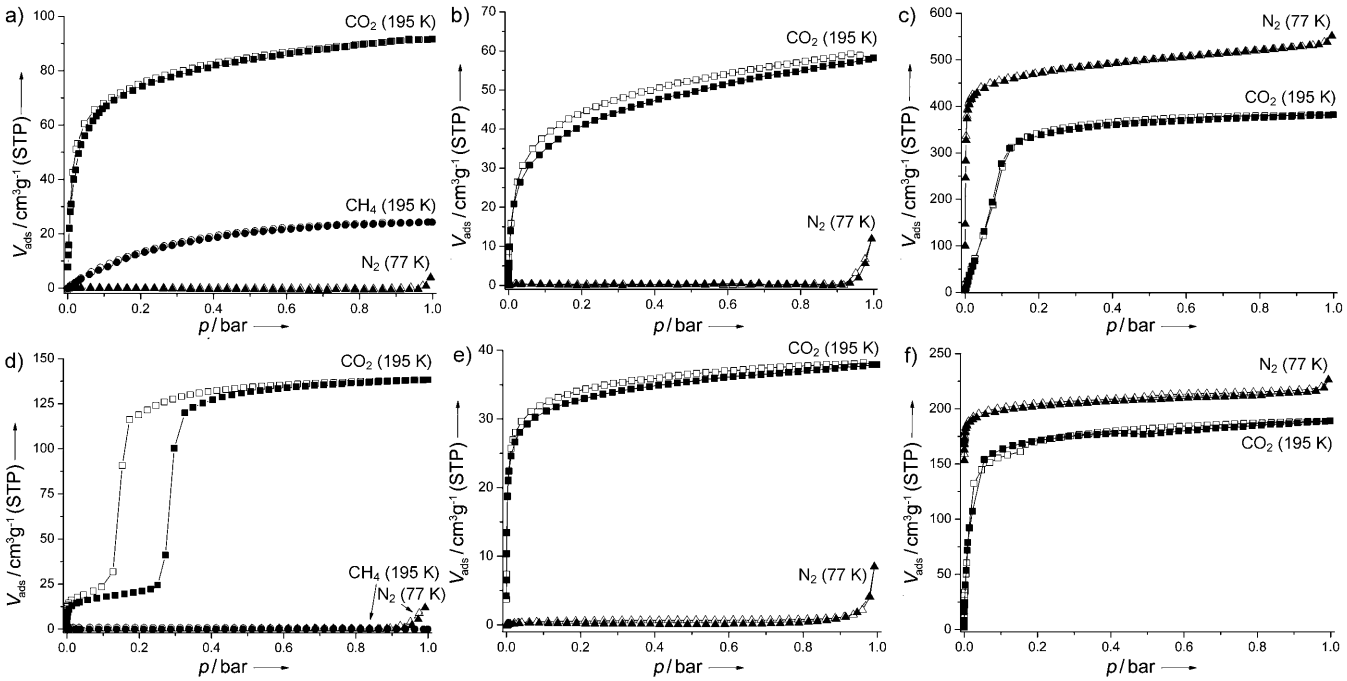

Figure 9. N_2 (77 K, ▲), CO_2 (195 K, ■) and CH_4 (195 K, ●) sorption isotherms of a) $[Zn_4O(L^1)_3]_n$; b) $[Zn_4O(L^2)_3]_n$; c) $[Zn_4O(L^4)_3]_n$; d) $[Zn_2(L^1)_2(dabco)]_n$; e) $[Zn_2(L^2)_2(dabco)]_n$ and f) $[Zn_2(L^4)_2(dabco)]_n$. CH_4 sorption isotherms were only recorded for the materials $[Zn_4O(L^1)_3]_n$ and $[Zn_2(L^1)_2(dabco)]_n$. The adsorption and desorption branches are shown with closed and open symbols, respectively.

$[Zn_2(L^1)_2(dabco)]_n$ and $[Zn_2(L^2)_2(dabco)]_n$ adsorb CO_2 easily, but N_2 is not able to penetrate into the pores. In fact, there is no uptake of nitrogen at all. This behaviour can only be attributed to the presence of methoxy groups in the functionalised materials. Note, that IRMOF-4 and IRMOF-5, which are very similar to $[Zn_4O(L^1)_3]_n$ and $[Zn_4O(L^2)_3]_n$, display permanent porosity towards N_2 and no CO_2 sorption selectivity.[1] The only difference is the methoxy group at the end of the alkyl chain in the functionalised MOFs instead of a simple alkyl chain in IRMOF-4 and IRMOF-5. Therefore, the reason for the high selectivity of the functionalised materials is not the reduction of the pore aperture window size (e.g., a molecular sieving effect), but the very polar methoxy-terminated pore surface.

Compared with the loading with polar solvents, in situ PXRD of amorphous $[Zn_4O(L^1)_3]_n$ at 195 K in CO_2 atmosphere (1 bar) does not show reordering of the structure and recovery of the crystalline state (data not shown). This data indicates that interesting sorption properties can very well be achieved with suitable coordination polymers, even in the case of an amorphous, non-crystalline phase. Thus, high crystalline order of MOFs is not a stringent prerequisite for porosity and high sorption selectivity.

The CO_2 sorption isotherms of the materials $[Zn_4O(L^1)_3]_n$, $[Zn_4O(L^2)_3]_n$ and $[Zn_2(L^2)_2(dabco)]_n$ exhibit a typical type I behaviour, whereas the CO_2 isotherm of $[Zn_2(L^1)_2(dabco)]_n$ is different. It displays a two-step uptake, which is typical for flexible MOFs that undergo a crystal-to-crystal transition upon adsorption. As already evident from the PXRD pattern, the dried $[Zn_2(L^1)_2(dabco)]_n$ exists in a narrow-pore state, which has only minor porosity. In the pressure range of $p = 0$–0.23 bar a typical type I isotherm behaviour is present. At the gate-opening pressure ($p = 0.23$ bar), the structure switches to the open state and the pores are rapidly filled with CO_2. On desorption a significant hysteresis is present with a gate-closing pressure of $p = 0.16$ bar.

In contrast, the materials $[Zn_4O(L^4)_3]_n$ and $[Zn_2(L^4)_2(dabco)]_n$ do not possess any sorption selectivity (Figure 9c and f, respectively). Both gases, N_2 and CO_2, are almost equally adsorbed in these materials. Determination of the specific surface area from the nitrogen sorption isotherms according to the BET model yields surface areas of 1730 $m^2 g^{-1}$ for $[Zn_4O(L^4)_3]_n$ ($S_{Langmuir} = 2130\ m^2 g^{-1}$) and 810 $m^2 g^{-1}$ $[Zn_2(L^4)_2(dabco)]_n$ ($S_{Langmuir} = 895\ m^2 g^{-1}$). These values are significantly lower than the surface areas of the unmodified parent structures $[Zn_4O(bdc)_3]_n$ and $[Zn_2(bdc)_2(dabco)]_n$.[8,15] This can be ascribed to the additional functional groups localised in the framework voids, which increase molecular weight and density, and decrease the accessible free volume compared with the unmodified parent structures. Remarkably, the CO_2 sorption capacity of $[Zn_2(L^1)_2(dabco)]_n$ (140 $cm^3 g^{-1}$ at 1 bar) and $[Zn_2(L^4)_2(dabco)]_n$ (180 $cm^3 g^{-1}$ at 1 bar) is very similar. However, the nitrogen sorption capacity is very different (almost 0 $cm^3 g^{-1}$ for $[Zn_2(L^1)_2(dabco)]_n$ and 200 $cm^3 g^{-1}$ for $[Zn_2(L^4)_2(dabco)]_n$). This underlines the important influence of the substitution pattern at the bdc-type linkers.

Furthermore, CH_4 sorption isotherms recorded on the materials $[Zn_4O(L^1)_3]_n$ and $[Zn_2(L^1)_2(dabco)]_n$ show interesting results (Figure 9). CH_4 is still able to penetrate in the pores of $[Zn_4O(L^1)_3]_n$. Nevertheless, the uptake of CH_4 is much less compared to CO_2 at the same temperature (selectivity factor $= V_{ads}(CO_2)/V_{ads}(CH_4) = 3.78$ at 1.0 bar). Because there is no uptake of N_2 in $[Zn_4O(L^1)_3]_n$, the material is promising for highly selective separation of CH_4 and N_2, which is a rarely reported feature of MOFs.[25] In contrast, $[Zn_2(L^1)_2(dabco)]_n$ shows essentially no uptake of CH_4 and N_2, which makes it highly selective for the adsorption of CO_2 (Figure 10).

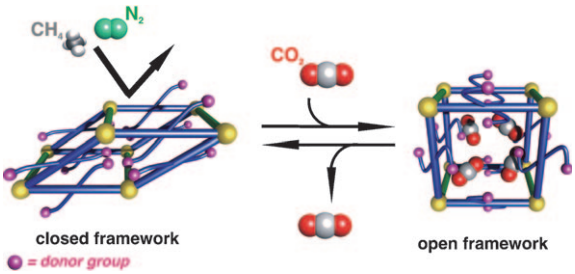

Figure 10. Sketch of the selective sorption in $[Zn_2(L^1)_2(dabco)]_n$. CH_4 and N_2 cannot enter the pores in the closed state and will not be adsorbed in the functionalised MOF, whereas CO_2 as able to penetrate in the pores and transform the structure to the open state.

Conclusion

Our data demonstrate the potential of alkyl ether functionalised linkers to tune flexibility and sorption properties of MOFs. The alkyl ether chain length has a huge influence on the structural flexibility of the materials. Both MOFs that utilise linker L^1 show remarkable flexibility and structural transformations in response to adsorbed guest molecules that are not so extensive in the related materials, which utilise linkers with longer alkyl ether chains (L^2 and L^3). Furthermore, the substitution pattern of the bdc-type linker has a critical impact on the sorption properties of the presented materials. In general, the materials utilising a bdc derivative substituted in positions 2 and 5 (linkers L^1 and L^2) exhibit high sorption selectivity towards CO_2, whereas the materials employing the bdc derivative only substituted in position 2 (linker L^4) do not.

Clearly, the density of flexible ether groups in the framework is of high significance. We suggest that the flexible and polar groups act as molecular gates at the pore apertures of the porous networks. At least two flexible ether chains per dicarboxylate linker are necessary to lock the pore windows effectively. Due to the polar nature of the ether chains, polar molecules such as CO_2 can easily penetrate through the molecular gate, whereas N_2 molecules cannot. We would like to emphasise here that even an amorphous MOF phase, such as $[Zn_4O(L^1)_3]_n$, may exhibit interesting sorption properties. Perfect long-range translational order of the MOF material and/or reversible crystalline-to-crystalline transfor-

mations as in the case of $[Zn_2(L^1)_2(dabco)]_n$ is apparently not a general prerequisite for highly selective gas adsorption for (functionalised) porous coordination polymers. Rather, the sorption properties of the discussed functionalised MOFs are mainly dependent on the particular linkers and only weakly dependent on the details of the framework structure. Therefore, it should in principle be possible to tune the sorption properties of MOFs in general by rational design of suitably functionalised linkers.

In summary, we have developed a methodology to integrate responsiveness and flexibility accompanied with high sorption selectivity towards CO_2 in already known, otherwise quite rigid, MOFs without changing the underlying reticular structure type and topology. We use the quite abundant bdc-type linkers, which were covalently modified with flexible alkyl ether side chains that do not interfere with MOF formation and are thus likely to be widely applicable in the synthesis of other bdc-based MOF systems. According to multivariate MOFs, which were recently introduced by Deng et al., it should in principle be possible to fine-tune sorption selectivity and flexibility of MOFs by utilising several ether-functionalised and non-functionalised linkers in varying ratios in MOF synthesis.[20b] In future work we will examine if related and similarly functionalised carboxylate linkers can establish sorption selectivity and structural flexibility in such multivariant and other related MOF structures.

Experimental Section

Materials: All chemicals were purchased from commercial suppliers (Sigma–Aldrich, Fluka, Alfa Aesar, and others) and used without further purification. THF used in the linker synthesis was catalytically dried, deoxygenated, and saturated with argon using an automatic solvent purification system from MBraun. The residual water content was determined by Karl Fischer titration, exhibiting levels of 5 ppm. Before further manipulations all dried and activated MOF samples were stored under inert gas atmosphere in a glovebox.

Methods: Elemental analyses were performed in the Microanalytical Laboratory of the Department of Analytical Chemistry at the Ruhr-University Bochum. Liquid-phase NMR spectra were recorded on a Bruker Advance DPX-250 spectrometer (^{1}H, 250.1 MHz; ^{13}C, 62.9 MHz) at 293 K. ^{1}H NMR spectra of the synthesised linker molecules were recorded in [D$_8$]THF, whereas the ^{1}H and ^{13}C NMR spectra of the digested MOFs were recorded in 0.5 mL [D$_6$]DMSO and 0.1 mL DCl(20%)/D$_2$O. Chemical shifts are given relative to TMS and were referenced to the solvent signals as internal standards. Solid-state ^{13}C-MAS-NMR spectra were recorded on a Bruker DSX-400 MHz spectrometer in ZrO_2 rotors of 2.5 mm diameter at 293 K. All spectra were measured by applying pulse programs written by H.-J. Hauswald at the Department of Analytical Chemistry of the Ruhr-University Bochum. Several ^{13}C-MAS-NMR spectra show a rather weak signal at $\delta = 80$ ppm, which is a measurement artefact and can be assigned to the centre of the resonance experiment. IR spectra were recorded inside a glovebox on a Bruker Alpha-P FTIR instrument in the ATR geometry with a diamond ATR unit. Single-crystal X-ray structures were measured on an Oxford Excalibur 2 diffractometer in a nitrogen cold stream (100–110 K) using $Mo_{K\alpha}$ radiation ($\lambda = 0.71073$ Å). The structure was solved by direct methods using SHELXS-97 and refined against *F*2 on all data by full-matrix least squares with SHELXL-97 (SHELX-97 program package, Sheldrick, Universität Göttingen, 1997). The structures were treated with the "sqeeze" protocol in the PLATON program package to give an account for the electron density associated to the disordered alkyl ether substituents, as well as disordered and partially occupied solvent molecules (DMF) in the porous coordination polymers. Powder X-ray diffraction (PXRD) patterns were recorded on a D8 Advance Bruker AXS diffractometer with $Cu_{K\alpha}$ radiation ($\lambda = 1.54178$ Å) and a Göbel mirror in θ–2θ geometry with a position-sensitive detector in a 2θ range from 5–50° at a scan speed of 1° min^{-1} at 298 K. α-Al_2O_3 was employed as an external standard. The powder sample of the as-synthesised MOF was filled into glass capillaries (diameter = 1.5 mm) with a pipette in air, whereas the samples of the dried and infiltrated materials were filled into glass capillaries (diameter = 0.7 mm) in a glovebox (Ar atmosphere). Each capillary was sealed prior to the measurement. The thermogravimetric analyses were performed on a Seiko TG/DTA 6300S11 instrument (sample weight approximately 10 mg) at a heating rate of 5 K min^{-1} in a temperature range from 300–870 K. The measurement was performed at atmospheric pressure under flowing nitrogen (99.9999%; flow rate = 300 mL min^{-1}). Sorption measurements were performed by using a Quantachrome Autosorp-1 MP instrument and optimised protocols and gases of 99.9995% purity. The N_2 measurements were performed at 77 K and CO_2 and CH_4 measurements at 195 K. XANES and EXAFS spectra were recorded at beamline X1 at HASYLAB, and Deutsches Elektronensynchrotron DESY, Hamburg, using a Si(111) double crystal monochromator (50% detuning for removing higher harmonics) and Zn-foil as reference. The data treatment was performed with the Winxas 3.1. software.[26]

Synthesis of 2,5-bis(2-methoxyethoxy)-1,4-benzene dicarboxylic acid (H_2L^1): The functionalised linkers were synthesised by Mitsunobu etherification.[16] Diethyl 2,5-dihydroxyterephthalate (1.12 g, 4.42 mmol), triphenylphosphine (2.43 g, 9.30 mmol), and di-*tert*-butylazodicarboxylate (2.14 g, 9.30 mmol) were suspended in dry THF (15 mL). 2-Methoxyethanol (9.30 mmol) was added dropwise to the solution. Subsequently, the reaction mixture was stirred and sonicated for 10 min and then washed with hexane (2 mL). NaOH (0.30 g) in water (10 mL) was added to the ether phase followed by 60 min sonication. Accordingly the water phase was separated from the ether phase and extracted three times with ethyl acetate. Finally the water phase was acidified with aqueous HCl ($\approx$10%) and the precipitated white product was filtered, recrystallised from methanol and dried in vacuo to give H_2L^1 (1.25 g, 3.98 mmol, 90%). ^{1}H NMR (250 MHz, [D$_8$]THF, 25 °C, TMS): $\delta = 7.58$ (s, 2H; Ar-H), 4.23 (t, 4H; CH_2), 3.71 (t, 4H; CH_2), 3.38 ppm (s, 6H; CH_3).

Synthesis of 2,5-bis(3-methoxypropoxy)-1,4-benzene dicarboxylic acid (H_2L^2): Diethyl 2,5-dihydroxyterephthalate (1.12 g, 4.42 mmol), triphenylphosphine (2.43 g, 9.30 mmol), and di-*tert*-butylazodicarboxylate (2.14 g, 9.30 mmol) were suspended in dry THF (15 mL). 3-Methoxypropanol (9.30 mmol) was added dropwise to the solution. Subsequently, the reaction mixture was stirred and sonicated for 10 min and then washed with hexane (2 mL). NaOH (0.30 g) in water (10 mL) was added to the ether phase followed by 60 min sonication. Accordingly the water phase was separated from the ether phase and extracted three times with ethyl acetate. Finally the water phase was acidified with aqueous HCl ($\approx$10%) and the precipitated white product was filtered, recrystallised from methanol and dried in vacuo to give H_2L^2 (1.29 g, 3.78 mmol, 85%). ^{1}H NMR (250 MHz, [D$_8$]THF, 25 °C, TMS): $\delta = 7.51$ (s, 2H; Ar-H), 4.14 (t, 4H; CH_2), 3.54 (t, 4H; CH_2), 3.28 (s, 6H; CH_3), 2.01 ppm (m, 2H; CH_2).

Synthesis of 2,5-bis(4-methoxybutoxy)-1,4-benzene dicarboxylic acid (H_2L^3): Diethyl 2,5-dihydroxyterephthalate (1.12 g, 4.42 mmol), triphenylphosphine (2.43 g, 9.30 mmol), and di-*tert*-butylazodicarboxylate (2.14 g, 9.30 mmol) were suspended in dry THF (15 mL). 4-Methoxybutanol (9.30 mmol) was added dropwise to the solution. Subsequently, the reaction mixture was stirred and sonicated for 10 min and then washed with hexane (2 mL). NaOH (0.30 g) in water (10 mL) was added to the ether phase followed by 60 min sonication. Accordingly the water phase was separated from the ether phase and extracted three times with ethyl acetate. Finally the water phase was acidified with aqueous HCl ($\approx$10%) and the precipitated white product was filtered, recrystallised from methanol and dried in vacuo to give H_2L^3 (1.33 g, 3.59 mmol, 81%). ^{1}H NMR (250 MHz, [D$_8$]THF, 25 °C, TMS): $\delta = 7.48$ (s, 2H; Ar-H), 4.07 (t, 4H; CH_2), 3.39 (t, 4H; CH_2), 3.26 (s, 6H; CH_3), 1.85 ppm (m, 4H; CH_2).

Synthesis of 2-(2-methoxyethoxy)-1,4-benzene dicarboxylic acid (H_2L^4): The precursor 2-hydroxyterephthalic acid was synthesised according to a literature report.[27] 2-Bromoterephthalic acid (5.00 g, 20.4 mmol), NaOH (1.64 g, 40.8 mmol) and NaOAc (3.68 g, 44.8 mmol) were dissolved in water (95 mL). Cu powder (0.026 g) and few drops of phenolphthalein solution were added and the mixture was heated under reflux for 4 d. Occasionally aqueous KOH (≈10%) was added to keep the reaction mixture alkaline. After cooling, the mixture was filtered, and the filtrate was acidified with aqueous HCl (≈10%). A white solid precipitated, was collected by filtration and dried in vacuo to give 2-hydroxyterephthalic acid (3.52 g, 19.3 mmol, 95%). The 2-hydroxyterephthalic acid was used without further purification. 2-Hydroxyterephthalic acid (3.52 g, 19.3 mmol) was dissolved in dry methanol (50 mL) and borontrifluoride ethyl etherate (5 mL). Afterwards the solution was heated at reflux for 2 h and then cooled to room temperature. The solvent was completely removed under reduced pressure. The white residue was washed three times with water, recrystallised from pyridine and dried in vacuo to give dimethyl 2-hydroxyterephthalate. Etherification of the hydroxyl group was again performed according to the Mitsunobu method.[16] Dimethyl 2-hydroxyterephthalate (1.00 g, 4.76 mmol), triphenylphosphine (1.31 g, 5.00 mmol), and di-*tert*-butylazodicarboxylate (1.15 g, 5.00 mmol) were suspended in dry THF (10 mL). 2-methoxyethanol (5.00 mmol) was added dropwise to the solution. The reaction mixture was stirred and sonicated for 10 min and then extracted with hexane (2 mL). NaOH (0.40 g) in water (10 mL) was added to the ether phase followed by 60 min sonication. Accordingly the water phase was separated from the ether phase and extracted three times with ethyl acetate. Finally the water phase was acidified with aqueous HCl (≈10%) and the precipitated white product was filtered, recrystallised from methanol and dried in vacuo to give H_2L^4 (0.989 g, 4.12 mmol, 87%). ^{1}H NMR (250 MHz, [D$_8$]THF, 25 °C, TMS): $\delta = 7.87$ (d, 1H; Ar-H), 7.73 (s, 1H; Ar-H), 7.65 (d, 1H; Ar-H), 4.29 (t, 2H; CH_2), 3.76 (t, 2H; CH_2), 3.41 ppm (s, 3H; CH_3).

Synthesis of $[Zn_4O(L^X)_3]_n$ (X=1, 2, 3 and 4): H_2L^X (X=1, 2, 3 and 4; 0.666 mmol) and $Zn(NO_3)_2{\cdot}4H_2O$ (0.756 g, 2.88 mmol) were dissolved in DMF (50 mL). The reaction mixture was transferred into a 100 mL reaction vessel, sealed and heated from room temperature to 373 K with a heating rate of 2 K h^{-1}. The target temperature was held for 20 h. Then the vessel was cooled to room temperature with a rate of −1.5 K h^{-1}. Subsequently, the mother liquor was decanted and the colourless, cubic MOF crystals of $[Zn_4O(L^X)_3(DMF)_m]_n$ (X=1, 2, 3 and 4) were washed three times with DMF and then stored in DMF (30 mL) until further manipulation was required. The as-synthesised materials were characterised by single-crystal X-ray diffraction analysis, PXRD and IR spectroscopy. The DMF was decanted off and the crystals were stirred for 3 d in chloroform (50 mL), whereas every 24 h the solvent was replaced by fresh $CHCl_3$. Afterwards the materials were dried under reduced pressure (≈10^{-3} mbar) for 48 h at 400 K to achieve the dried MOFs $[Zn_4O(L^X)_3]_n$ (X=1, 2, 3 and 4), which were stored under inert gas atmosphere in a glovebox. The dried MOFs were characterised by elemental analysis, PXRD, N_2 and CO_2 sorption, thermogravimetric analysis, IR and ^{13}C-MAS-NMR spectroscopy. Further characterisation was performed by digestion of a few milligrams in [D$_6$]DMSO (0.5 mL) and DCl (0.1 mL)/D_2O (20%) and collection of ^{1}H and ^{13}C NMR spectra.

Synthesis of $[Zn_2(L^X)_2(dabco)]_n$ (X=1, 2, 3 and 4): The materials were synthesised in analogy to the literature synthesis of $[Zn_2(bdc)_2(dabco)]_n$.[15] $Zn(NO_3)_2{\cdot}6H_2O$ (500 mg, 1.68 mmol), H_2L^X (X=1, 2, 3 and 4; 1.68 mmol), and 1,4-diazabicyclooctane (0.094 g, 0.84 mmol) were suspended in DMF (20 mL) and transferred into a 50 mL reaction vessel. The mixture was heated to 393 K for 48 h to yield block-shaped colourless crystals of $[Zn_2(L^1)_2(dabco)(DMF)_m]_n$ or a microcrystalline powder material of $[Zn_2(L^X)_2(dabco)(DMF)_m]_n$ (X=2, 3 and 4). After cooling to room temperature the material was washed twice with fresh DMF. The as-synthesised materials were characterised with PXRD and IR spectroscopy. The crystals of $[Zn_2(L^1)_2(dabco)(DMF)_m]_n$ were further analysed by single-crystal X-ray diffraction. For activation the materials were stirred in chloroform (50 mL) for 3 d, followed by filtration and drying under reduced pressure (≈10^{-3} mbar) at 400 K for 48 h. Characterisation of the dried materials $[Zn_2(L^X)_2(dabco)]_n$ (X=1, 2, 3 and 4) was performed with elemental analysis, PXRD, thermogravimetric analyses, IR and ^{13}C-MAS-NMR spectroscopy and ^{1}H and ^{13}C NMR spectroscopy of digested samples in [D$_6$]DMSO (0.5 mL) and DCl (0.1 mL)/D_2O (20%). For analyses of the sorption properties of the materials N_2 and CO_2 sorption isotherms were recorded.

Gas-phase infiltration of solvent guests in the dried donor-functionalised MOFs: In a typical infiltration experiment the dedicated material $[Zn_4O(L^X)_3]_n$ or $[Zn_2(L^X)_2(dabco)]_n$ (X=1, 2, 3 and 4; 100 mg) and the solvent guests (DMF, DEF, THF, EtOH, toluene or pentane; 1 mL) were placed in two separate glass vials in a Schlenk tube. The tube was evacuated for 1 min to achieve a static vacuum, sealed and kept at room temperature (323 K for DMF, DEF, and toluene) for 16 h to achieve the maximum loading of the material. The infiltrated materials guest@$[Zn_4O(L^X)_3]_n$ and guest@$Zn_2(L^X)_2(dabco)]_n$ (X=1, 2, 3 and 4) were stored under an inert atmosphere. PXRD was carried out for characterisation.

CCDC-788015, 788016, 788017, 788018 and 788019 contain the supplementary crystallographic data for this paper. These data can be obtained free of charge from The Cambridge Crystallographic Data Centre via www.ccdc.cam.ac.uk/data_request/cif.

Acknowledgements

The authors would like to thank the "Research Centre 558" of the German Research Foundation DFG for funding. S.H. is grateful to acknowledge the Research School of the Ruhr-University Bochum for a fellowship and the "Fonds of the German Chemical Industry" for a doctoral scholarship. We thank HASYLAB at DESY (Hamburg, Germany) for beamtime allocation and the EU for financial support (contract RII3-CT-2004-506008).

[1] M. Eddaoudi, J. Kim, N. Rosi, D. Vodak, J. Wachter, M. O'Keeffe, O. M. Yaghi, *Science* **2002**, *295*, 469–472.
[2] a) S. Kitagawa, R. Kitaura, S. Noro, *Angew. Chem.* **2004**, *116*, 2388–2430; *Angew. Chem. Int. Ed.* **2004**, *43*, 2334–2375; b) R. Robson, *Dalton Trans.* **2008**, 5113–5131.
[3] a) A. R. Millward, O. M. Yaghi, *J. Am. Chem. Soc.* **2005**, *127*, 17998–17999; b) M. Dinca, J. Long, *Angew. Chem.* **2008**, *120*, 6870–6884; *Angew. Chem. Int. Ed.* **2008**, *47*, 6766–6779.
[4] M. D. Allendorf, R. J. T. Houk, L. Andruszkiewicz, A. A. Talin, J. Pikarsky, A. Choudhury, K. A. Gall, P. J. Hesketh, *J. Am. Chem. Soc.* **2008**, *130*, 14404–14405.
[5] a) L. Alaerts, C. E. A. Kirschhock, M. Maes, M. A. van der Veen, V. Finsy, A. Depla, J. A. Martens, G. V. Baron, P. A. Jacobs, J. F. M. Denayer, D. E. De Vos, *Angew. Chem.* **2007**, *119*, 4371–4375; *Angew. Chem. Int. Ed.* **2007**, *46*, 4293–4297; b) J.-R. Li, R. J. Kuppler, H.-C. Zhou, *Chem. Soc. Rev.* **2009**, *38*, 1477–1504, and references therein.
[6] J. Y. Lee, O. K. Farha, J. Roberts, K. A. Scheidt, S. T. Nguyen, J. T. Hupp, *Chem. Soc. Rev.* **2009**, *38*, 1450–1459.
[7] P. Horcajada, C. Serre, G. Maurin, N. A. Ramsahye, F. Balas, M. Vallet-Regí, M. Sebban, F. Taulelle, G. Férey, *J. Am. Chem. Soc.* **2008**, *130*, 6774–6780.
[8] H. Li, M. Eddaoudi, M. O'Keefe, O. M. Yaghi, *Nature* **1999**, *402*, 276–278.
[9] D. Maspoch, D. Ruiz-Molina, K. Wurst, N. Domingo, M. Cavallini, F. Biscarini, J. Tejada, C. Rovira, V. Veciana, *Nat. Mater.* **2003**, *2*, 190–195.
[10] G. Férey, C. Serre, *Chem. Soc. Rev.* **2009**, *38*, 1380–1399.
[11] G. J. Halder, C. J. Kepert, B. Moubaraki, K. S. Murray, J. D. Cashion, *Science* **2002**, *298*, 1762–1765.
[12] C. Volkringer, S. M. Cohen, *Angew. Chem.* **2010**, *122*, 4748–4752; *Angew. Chem. Int. Ed.* **2010**, *49*, 4644–4648.
[13] Z. Wang, S. M. Cohen, *J. Am. Chem. Soc.* **2009**, *131*, 16675—16677.
[14] J. Seo, R. Matsuda, H. Sakamoto, C. Bonneau, S. Kitagawa, *J. Am. Chem. Soc.* **2009**, *131*, 12792–12800.
[15] D. Dybtsev, H. Chun, K. Kim, *Angew. Chem.* **2004**, *116*, 5143–5146; *Angew. Chem. Int. Ed.* **2004**, *43*, 5033–5036.

[16] a) O. Mitsunobu, *Synthesis* **1981**, 1; b) S. D. Lepore, Y. He, *J. Org. Chem.* **2003**, *68*, 8261–8263.
[17] Q. Li, W. Zhang, O. Miljani, C.-H. Sue, Y.-L. Zhao, L. Liu, C. B. Knobler, J. F. Stoddart, O. M. Yaghi, *Science* **2009**, *325*, 855–859.
[18] D. J. Tranchemontagne, J. R. Hunt, O. M. Yaghi, *Tetrahedron* **2008**, *64*, 8553–8557.
[19] a) S. Kitagawa, K. Uemura, *Chem. Soc. Rev.* **2005**, *34*, 109–119, and references therein; b) N. Yanai, W. Kaneko, K. Yoneda, M. Ohba, S. Kitagawa, *J. Am. Chem. Soc.* **2007**, *129*, 3496–3497; c) C.-D. Wu, W. Lin, *Angew. Chem.* **2005**, *117*, 1994–1997; *Angew. Chem. Int. Ed.* **2005**, *44*, 1958–1961.
[20] a) Z. Wang, S. M. Cohen, *Chem. Soc. Rev.* **2009**, *38*, 1315–1329; b) H. Deng, C. J. Doonan, H. Furukawa, R. B. Ferreira, J. Towne, C. B. Knobler, B. Wang, O. M. Yaghi, *Science* **2010**, *327*, 846–850.
[21] M. Eddaoudi, D. B. Moler, H. Li, B. Chen, T. M. Reineke, M. O'Keeffe, O. M. Yaghi, *Acc. Chem. Res.* **2001**, *34*, 319–330.
[22] V. Zelenák, Z. Vargová, K. Györyová, *Spectrochem. Acta Part A* **2007**, *66*, 262–272.
[23] a) A. D. Burrows, C. G. Frost, M. F. Mahon, C. Richardson, *Angew. Chem.* **2008**, *120*, 8610–8614; *Angew. Chem. Int. Ed.* **2008**, *47*, 8482–8486; b) A. P. Nelson, O. K. Farha, K. L. Mulfort, J. T. Hupp, *J. Am. Chem. Soc.* **2009**, *131*, 458–460.
[24] K. Uemura, Y. Yamasaki, Y. Komagawa, K. Tanaka, H. Kita, *Angew. Chem.* **2007**, *119*, 6782–6785; *Angew. Chem. Int. Ed.* **2007**, *46*, 6662–6665.
[25] a) K. Seki, *Phys. Chem. Chem. Phys.* **2002**, *4*, 1968–1971; b) R. Kitaura, K. Seki, G. Akiyama, S. Kitagawa, *Angew. Chem.* **2003**, *115*, 444–447; *Angew. Chem. Int. Ed.* **2003**, *42*, 428–431.
[26] T. Ressler, *J. Synchrotron Radiat.* **1998**, *5*, 118–122.
[27] Y. Miura, E. Torres, C. A. Panetta, R. M. Metzger, *J. Org. Chem.* **1988**, *53*, 439–440.

Received: August 15, 2010
Published online: December 7, 2010

